Arabian Journal of Chemistry (2020) 13, 7418–7429

King Saud University

Arabian Journal of Chemistry

www.ksu.edu.sa
www.sciencedirect.com

ORIGINAL ARTICLE

Porous nano-minerals substituted apatite/chitin/pectin nanocomposites scaffolds for bone tissue engineering

Yanchao Cui [a], Qiong Wu [a], Juan He [a], Meng Li [b], Zhi Zhang [b], Yusheng Qiu [b,*]

[a] Department of Rehabilitation Medicine, The First Affiliated Hospital of Xi'an Jiaotong University, Xi'an, China
[b] Department of Orthopaedics, The First Affiliated Hospital of Xi'an Jiaotong University, Xi'an, China

Received 29 June 2020; accepted 18 August 2020
Available online 27 August 2020

KEYWORDS

Apatite;
Chitin;
Cartilage;
Gallium;
Nanocomposites;
Pectin

Abstract In the current study, a porous 3D scaffold using Gallium-Apatite/chitin/pectin (Ga-HA/C/P) nanocomposites scaffolds (NCS) were fabricated by freeze-drying process with applications in orthopedics (bone tissue engineering). Various NCSs (0%, 30%, 50 and 70%) were prepared and characterized for its chemical structure, crystalline phase, surface texture by using various techniques such as FT-IR, XRD and SEM-EDX, respectively. The analyses of physicochemical properties proved that the formulated scaffolds were highly porous, and mechanically stable with superior density. The nanocomposite scaffolds also presented with increased swelling ability, lower biodegradation rate and higher mechanical strength. Further, biocompatibility and cytotoxicity of Ga-HA/C/P nanocomposite scaffolds were studied using NIH3T3 cells and MG-63 cells revealed no toxicity and cells attached and proliferated on scaffolds. Further implantation of prepared NCS showed mature bone formation through formation of new bone cells and osteoblast differentiation. Also, Ga-HA/C/P nanocomposites scaffolds proved to be more effective than chitin-pectin composite scaffolds. Taking results together it can be inferred that the prepared nanocomposite scaffolds possesses the prerequisites and showed great potential for treating orthopedic applications.

1. Introduction

Bone imperfections resulted from carcinomas, infections, injuries, biological complications, and atypical bony progress can cause serious health issues (Wu et al., 2018; Shea et al., 2000; Zhu et al., 2020; Qiu et al., 2020). Conventional biological approaches like reconstructing grafts (autografts or allografts) with synthetic macromolecule materials have been utilized to combat such imperfection issues (Dantas et al., 2011;

* Corresponding author.
E-mail address: yusheng.qiu@mail.xjtu.edu.cn (Y. Qiu).
Peer review under responsibility of King Saud University.

Production and hosting by Elsevier

https://doi.org/10.1016/j.arabjc.2020.08.018
1878-5352

Tiedeman et al., 1995; Cui et al., 2020). The cartilage reconstruction through tissue engineering essentially provides a suitable environment either to reconstruct or rejuvenate the infected or ailing tissues within the body (Williams, 1999; Bouler et al., 2017; Zhang et al., 2019a, 2019b). In the current scenario, a 3D porous biocompatible macromolecule scaffold has attracted the scientific attention which can allow cell attachment and also provide an arrangement for tissue reconstruction (Lee et al., 2014). The inclusion of extracellular network materials, augmentation features, and supplements plays an important role to ensure physicochemical characteristics of the scaffold convenient for the target tissue (Zhang et al., 2019c; Wang et al., 2019a, 2019b).

Hydroxy apatite (HA) is one such supplement that is nontoxic, bioactive, osteo-inductive, osteo-conductive and it also possesses low dissolvability in human body fluids and therefore it cannot be recovered by freshly developed cartilage tissues (Govindaraj et al., 2017). Furthermore, the novel strategy in the development of apatite is addition of different bioactive minerals to enhance the physicochemical and biochemical assets of apatite (Supova, 2015). Considering the presence of bioactive minerals in human cartilage tissues, it is believed to play an vital function in osteogenesis. Primarily, Gallium (Ga) bioactive minerals have been shown to promote the bioactivity of apatite bio-ceramics via promoting an augmented in vitro osteoblast cell propagation and adhesion (Melnikov et al., 2009; Kurtjak et al., 2016) and accounts for advanced biomedical applications. The gallium ions are possessed the positive effects on the bone cells via the stimulation of osteoblasts and defending from augmented resorption by inhibiting osteoclast activity and modifying the crystal solubility that is connected in the osteoporosis treatment (Chitambar, 2010; Nayak and Misra, 2020; Cassino et al., 2018). The pectins were established as a potent agent for the surface nanocoating of medical devices because of their effect on bone cells and possibility of controlling their structure (Bussy et al., 2008; Kokkonen et al., 2007). The effect on bone cells was explicated via a direct adhesion of cells to pectins and indirectly via proteins binding to the pectins (Gurzawska et al., 2012). Pectin nanocoating was elucidated in a various investigations to moderate the osteoblast response due to their physical and chemical assets (Morra et al., 2004).

Additionally, an interconnected porous arrangement is important to permit cell adhesion, propagation and to give conduit for body fluids. Pectin belongs to a class of plant polysaccharides comprises of a galacturonan backbone and neutral sugar side chains and shown to have wide range of commercial applications (Zhang et al., 2015). Earlier studies have highlighted the application of pectin-based scaffolds in orthopeadic, wound healing, genetic material carrying, medication release and malignancy targeting (Noreen et al., 2017). Commercially, pectin is derived from the apple, citrus, or other higher plant fruit peels. Since the price of pectin employed in enterprises is generally > USD 11/kg, numerous other ways such as extraction of pectin from natural product peels and pomace could offer new viable sources from substance that is otherwise eliminated (Banerjee et al., 2016).

Cashew trees (*Anacardium occidentale L.*), the significant sources of pectins are tropical evergreen trees that produces cashew fruits and nuts. India is a significant contributor in the production of cashews globally. Generally, nut production considers cashew fruits as an industrial waste and infection inoculum(Mohamed and Hasan, 1995), so therefore is essential to have a method in place to enhance profits to farmers and to prevent the ecological dilemma it induces.

Owing to impaired mechanical properties of pectin, it is usually combined with many other polymers. Chitin is a commonly known biopolymer that is found in abundance in exoskeletons of arthropods and crustaceans. It is comparable structurally to starch and functionally to keratin. Owing to chitins therapeutic potential in treating wounds and fighting bacterial infections, the efforts have been carried out to apply it for different purposes like wound bandage and as scaffolds in bone replacement for cartilage reconstruction (Usman et al., 2016). It is also reported that its mechanical property can be enhanced with the inclusion of apatite (Govindaraj et al., 2017). The chemical structure of chitin helps in enhanced hydrogen bonding between neighboring groups of polymers and contributes better stability to the chitin–polymer network.

In this current exploration, the fabrication and interpretation of the blended scaffolds composed of biodegradable polymers (pectin and chitin) with bioactive substance Ga-HA for prospective application as a cartilage substitute substance for patients with bone cancers was studied. Physicochemical properties of the prepared scaffolds were studied. In vitro characterization investigations like swelling test, biodegradation, protein adsorption assay, cytotoxicity and cell attachment studies were studied. Further, in vivo bone healing ability of prepared NCSs was studied.

2. Materials and methods

2.1. Materials

Chitin, Ca $(NO_3)_2{\cdot}4H_2O$, Ga $(NO_3)_3{\cdot}H_2O$, $(NH_4)_2HPO_4$, and NaOH were attained from Aldrich-Chemicals for fabrication of scaffold. Double distilled water was utilized during the experiments. All other chemicals used in the study were procured from local commercial sources.

2.2. Cashews fruits powder preparation

Cashew fruits were collected from producers and sellers in Cuddalore, Tamilnadu, India. Initially, fruits were drenched in boiling ethanol for 30 min, cooled to room temperature (RT) and cleansed with ethanol three times to exclude excess impurities, pigments and free sugars. The treated cashews fruits were dried at 60 °C until stable mass is attained and made into fine powder. This dried sample was called as alcohol insoluble solid preparation.

2.3. Extraction of pectin

Pectin extraction was done using the microwave extraction method. The solid to solvent percentage was altered to 1:25 (w/v). Pectin was extracted by immersing the alcohol insoluble solid in double distilled (DD) water. The combination in a closed visible glass pot was positioned at the middle of microwave oven with 300 W for 10 min. The isolated solid was filtered and washed with ethanol until the filtrate turns into colorless. The washed cashew fruit pectin was then dried at 40 °C overnight and grinded to make fine powder.

2.4. Preparation Ga-HA nanoparticles

Ga-HA nanoparticles were synthesized as per published literature (Pal et al., 2017). Briefly Ca (0.294 M) and Ga (0.126 M) were mixed in DD water for the appearance the mineral precursor; the pH was altered to 9.0 using NaOH solution. $(NH_4)_2HPO_4$ (0.24 M) was suspended in DD water to make a phosphate precursor. Subsequent to mixing, the obtained precipitate was put in a sonicator for 2 hrs at a frequency of 20 kHz to form a consistent mixture and then dried in a hot air oven at 100 °C. The dried nanoparticles were washed thrice with ethanol and DD water subsequently calcination for 4 hrs and sintering at 1000 °C for 2 hrs.

2.5. Preparation of nanocomposite scaffolds

Pectin hydrogel was included into chitin solution and sonicated for 2 hrs at room temperature. Ga-HA was then incorporated to polymer solution and sonicated for 6 hrs to disperse Ga-HA in pectin/chitin solution. The final solution was shifted to 96-well culture dishes and subsequently cooled to 0 °C for 18 hrs and −35 °C for 24 hrs and then freeze dried at −80 °C for 72 hrs. Scaffolds were rinsed in DD water to eliminate any un-reacted ions, freeze dehydrated and kept for further use. Further to study the effect of Ga-HA content, three composites were prepared as NCS-1, NCS-2 and NCS-3 (Table 1).

2.6. Physicochemical characterization nanocomposite scaffolds

The bending and stretching vibration of scaffolds was checked by Fourier Transform Infrared Spectroscopy [spectrum GX-1, PerkinElmer (USA)] within the wavelength of 400–4000 cm^{-1}. The phases were assessed by Bruker D8 X-ray diffraction (XRD) with a Cu-K x-ray radiation at a tube voltage of 40 kV, current of 40 mA, 20–60° scanning angle, and a scanning rate (2θ) of 0.02°. Elemental and morphological composition of nanocomposite scaffolds were acquired via scanning electron microscopy (SEM: JEOL JSM LV-5600) outfitted with an in-situ energy dispersive X-ray (EDX) spectrometer. Mechanical investigation of the scaffolds was carried out using Instron materials analysis instrument (Instron 3342) by a 500 N weight cell at a fractious head velocity of 10^{-3} mm/sec. A liquid dislocation technique was employed to assess the density and porosity of scaffolds. The overall density and porosity were estimated using the equation:

$$\text{Density} = W/(X_2 - X_3) \quad (1)$$

$$\text{Porosity} = (X_1 - X_3)/(X_2 - X_3) \quad (2)$$

Table.1 Composition of as-prepared samples.

Sample Code	Chitin (%)	Pectin (%)	Ga-HA (%)
NC-1	35	35	30
NC-2	25	25	50
NC-3	15	15	70

Where W = Weight of scaffold; X_1 = Known volume of ethanol; X_2 = Total volume of the ethanol and scaffold; X_3- = Residual ethanol volume.

2.7. In vitro characterization

2.7.1. Swelling test

Swelling test is considered to be an important property to measure percentage of water absorption in biodegradable materials. In this assay, the prepared scaffold (of size 1 × 1 cm^2) was immersed in PBS at pH 7.4 and 37 °C. The dry weights of the scaffolds were estimated before immersion (W_d) and wet weights were estimated after immersion for 24 h by removing surface adsorbed water through filter paper (W_w). The swelling ratio was determined using the following equation:

$$\text{Swelling ratio} = (W_w - W_d)/W_d \quad (3)$$

Where W_w and W_d corresponds to the wet and initial dry weights of the scaffolds, respectively.

2.7.2. In vitro biodegradation

The in vitro biodegradation of scaffold was analyzed in PBS-medium containing lysozyme at RT. The initial weight of the scaffolds was verified previous to submerging (W_0) into PBS. On standard intermissions (1, 4, 7, 14, 21 and 28 days), the specimens were eliminated from the PBS, cleaned with DD water and dehydrated weight is considered as W_t. The degradation was derived by the following equation:

$$\text{Mass loss} = (\text{Wo} - \text{Wt})/\text{Wo} - 100 \quad (4)$$

2.7.3. Protein adsorption assay

The protein adsorption capability of the scaffolds was inspected by using the BCA protein adsorption test. The scaffold was stored in minimum essential medium (MEM) for 4, 8 and 12 hrs. The optical density of the solution was taken at a wavelength of 570 nm determined via Elisa plate reader.

2.7.4. Cytotoxicity and cell attachment studies

Human osteoblast cell line (MG-63) and fibroblasts cell line (NIH3T3) were acquired from ATCC, USA, for cytocompatibility tests. Cells were maintained in MEM medium with 10% FBS and 1% penicillin/streptomycin and maintained at 37 °C temperature in a moistened environment containing 5% CO_2.

The cytocompatibility of as-prepared nanocomposite scaffolds was inspected using 3-[4,5-dimethylthiazol-2-yl]-2,5-iphe nyltetrazolium bromide (MTT) test. In brief, the cells were loaded at a density of 2 × 10^4 cells per well in 96-well plates containing the scaffolds. Further, the plates were incubated for 24 and 48 hrs at 37 °C in a humid atmosphere with 5% CO_2. Subsequent to 24 and 48 hrs, medium from the culture was measured at a wavelength of 570 nm and 600 nm by using Elisa plate reader. The scaffolds with cells were then stained using DAPI for 5 min and incubated at 4°C. Fluorescent microscope was used to view nuclear staining images the cells attached on scaffolds.

2.8. In-vivo animal studies

2.8.1. Surgical procedure

In order to inspect the bone healing capacity of the Ga-HA/C/P scaffold in rat model, in-*vivo* studies were executed in Wistar rats (n = 6) weighed from 200 to 250 g. All the procedures to be executed by the 'Principles of Laboratory Animal Care' (NIH) and rules of the laboratory animal care committee of Xi'an Jiaotong University (Animal ethical approval number: XJTULAC2020-1227). All the rats were maintained under well controlled environmental conditions such as temperature (22 ± 3 °C), light: dark cycle (12 hr: 12 hr). The animals were acclimatized for a period of 2 weeks before being used for actual experimentation. All rats were anesthetized by 20 mg/kg of ketamine and 2 mg/kg of xylazine via an intraperitoneal injection. Further, the rats were subjected to inhalation of 20% v/v isoflurane and propylene glycol mixture. The left-side hind leg of the rat was shaved neatly and scrubbed with 10% poviodine-iodine for implantation and avoiding any skin infection. Orthopedic drilling machine was used to create the hole of about 2 mm beneath the regular wash with PBS to avoid overheating during Ga-HA/C/P scaffold implantation. First three days after the surgery, all the rats were administered penicillin as an antibiotic to avoid the microbial contamination (Wu et al., 2018).

2.8.2. X-Ray analysis and histological analysis

After 1 day, 2 and 4 weeks of implant, all the rats were killed and their bone healing process was assessed by observing the construction of new bone tissues via soft X-ray. The bone tissues with Ga-HA/C/P composite scaffolds were cut carefully and engrossed in 20% neutral formalin, decalcified with 10% acetic acid and embedded in paraffin. Then tissues were sliced at 5 μm portions, and then stained with Masson's trichrome and Hematoxylin & Eosin (H&E) staining to examine the structural modifications of newly formed bone tissues. All the images were inspected beneath the optical microscope (Olympus, Tokyo, Japan) at the 40× magnification.

2.8.3. Statistical analysis

Results were analyzed through the SPSS software version 18. Data were displayed as mean ± SD of triplicate tests. The one way ANOVA subsequently DMRT study was used to analyze the variations between groups. A *p*-value less than 0.05 regarded as significant.

3. Results

3.1. FT-IR spectrum

The FT-IR spectrum of Ga-HA displayed bands at 3430, 1042, 602 & 567 cm^{-1}, which were related to OH^- and PO_4^{3-} bending and stretching vibration modes correspondingly (Fig-1A) (Guolin et al., 2012). The spectra of pectin exhibited bands at 3428, 2919, 1749 and 1445 cm^{-1} which can be accredited to vibrations of the O—H (stretching), C—H (stretching), O═C—O structures (Fig. 1B) (Zhang et al., 2018). Additionally, the spectrum of chitin exposed bands at 3430, 1610 and 1396, which were dispensed to OH^- (stretching), amide I and C—CH_3 (bending) vibration mode separately (Fig. 1C) (Yang et al., 2011). FT-IR spectra of pectin–chitin scaffolds disclosed presence of band at 1647 cm^{-1} which agree to the primary amide groups of chitins (Fig. 1D). Equally, no particular bands were developed which could be owed to no biochemical response trendy between pectin–chitin scaffolds.

Fig. 1 (E-F) exemplifies the FT-IR spectra of NCS-1, NCS-2 and NCS-3 bio-composite frameworks. All the bio-composite scaffolds showed the consistent bands of PO_4^{3-} vibration at 1042 cm^{-1}, which designated the existence of nano-hydroxyapatite (n-HA) on the outward of bio-composite scaffolds. The strength of bands at 570 and 605 cm^{-1} augmented from (e-f), since the concentration of Ga-HA increased. For all scaffolds, the bands at 1662 cm^{-1} can be qualified to carboxylic acid (COOH) groups of pectin in Ga-HA/C/P. Carboxylic acid of pectin in Ga-HA/C/P occurs in the form of COO^- and the ionic bond between calcium carboxylate could be developed. As of spectrum (e–f), it was recognized that adding of Ga-HA into b-chitin lead to the broadening of the bands at 3440 cm^{-1}, which portrays the intermolecular hydrogen communication among amine chitin group and hydroxyl group of apatite.

3.2. Phase analysis

Fig. 2 validates the XRD patterns of organized pure Ga-HA and bio-composite scaffolds. Intense diffractions imitated to (321), (310), (202), (222), (213), (002), (300), (112) and (211) signs of Ga-HA phase, consistently. Further, admirable concurrence with the distinctive XRD patterns of HA (File No. 09-0432, JCPDS) (Hannink and Arts, 2011). The X-ray diffraction of the scaffolds mineralized for dissimilar time periods are depicted in Fig. 2. All the outlines look comparable and display an intense reflection with a wide peak around 30° presenting that, pectin molded on chitosan complex is apatite in assembly and no other phases like tricalcium phosphate was noticed. The peak is wider and well determined, because of the nano-crystalline nature of the apatite because of the shapeless layer of the framework. The broad peak at 3θ = 30° is an added contribution of the (211) and (300) lattice planes of apatite and pectin. This specifies Ga-HA was contained of well-developed crystals. The NC-1, NC-2 and NC-3 scaffolds signify the stages at the identical point, mentioned totally to unvarying phase crystalline Ga-HA, since no deflection points from other apatite phases were experiential. This indicates that the presence of biopolymers did not alter the crystalline development of Ga-HA.

3.3. Morphological analysis by SEM

Fig. 3 establishes the SEM photomicrographs of the arranged composite samples. In pure Ga-HA nanoparticles displays spherical shape with particle sizes extending from ~70–100 nm (Fig. 3a). In this bio-composite scaffolds, exposed interrelated pores could progress body fluid transmission and local tissue proliferation (Fig. 3b-d). As it can be experiential in Fig. 3(c-e), the upsurge in the Ga-HA constituent leads to the expansion in the quantity of pores. The alteration of minerals, cells, nutrients and oxygen was even sustained through pores in spite of the boundary amongst the macromolecule arrangements.

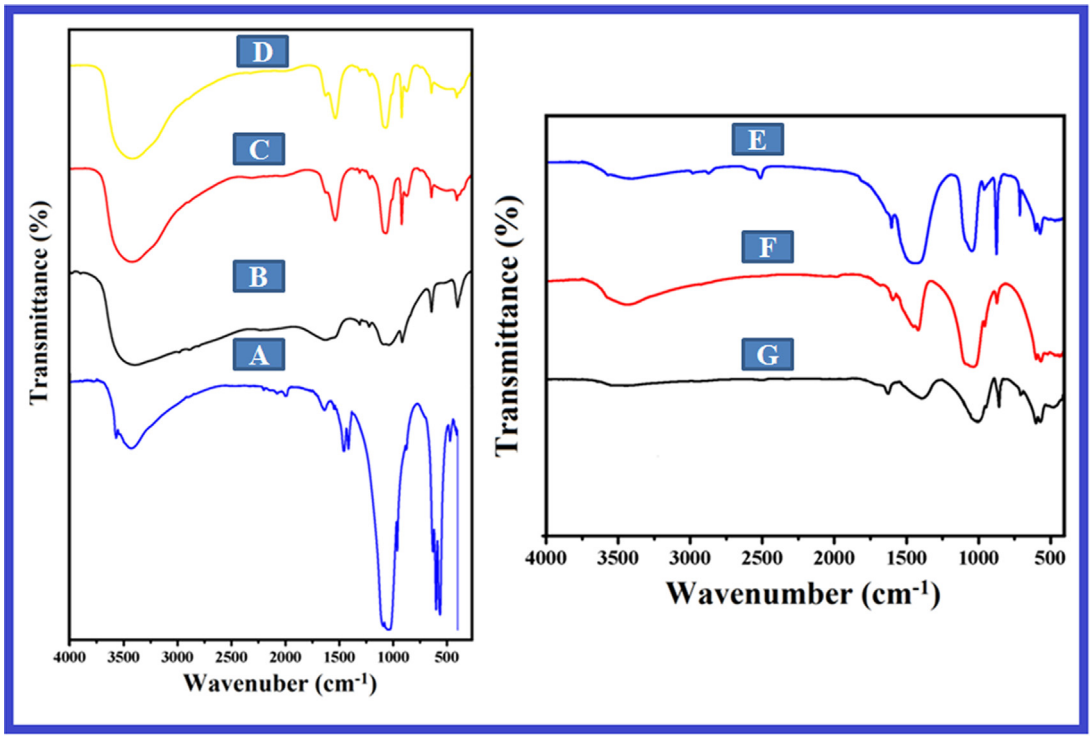

Fig.1 FT-IR spectra of (A) Ga-HA nanoparticles (B) Pectin isolated from the peels of cashews fruits (C) Chitin (D) Pectin- chitin (E) NC-1 (F) NC-2 and (G) NC-3 bio-nanocomposites. The FT-IR spectrum of Ga-HA displayed the presence of OH^{-} and PO_4^{3-}, O—H (stretching), C—H (stretching), O═C—O structures, amide I and C—CH_3 (bending). FT-IR spectra of pectin–chitin scaffolds disclosed presence of primary amide groups of chitins. FT-IR spectra of NCS-1 (E), NCS-2 (F) and NCS-3 (G) showed the existence of nano-hydroxyapatite (n-HA) on the outward of bio-composite scaffolds.

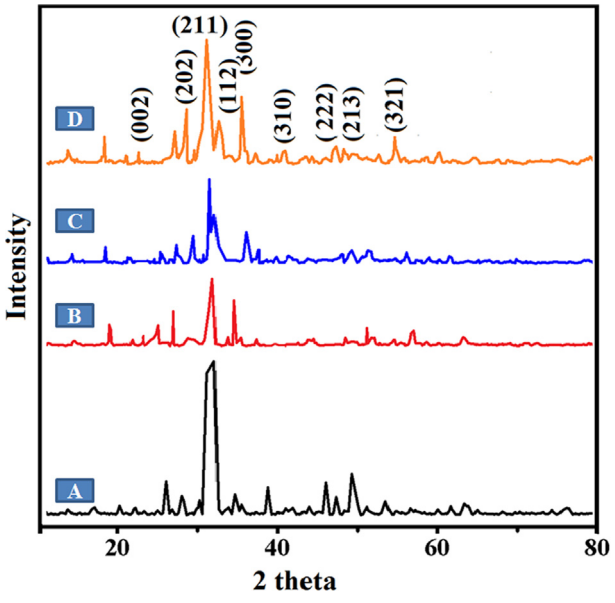

Fig. 2 XRD patterns of (A) Ga-HA (B) NC-1 (C) NC-2 and (D) NC-3 nanocomposites. Fig. 2 validates the XRD patterns of organized pure Ga-HA and bio-composite scaffolds. The broad peaks specifies Ga-HA was contained of well-developed crystals. The NC-1, NC-2 and NC-3 scaffolds signify the stages at the identical point, mentioned totally to unvarying phase crystalline Ga-HA.

3.4. Porosity and density

The porosity of the organized bio-composite scaffolds is pragmatic in Fig. 4A When the Ga-HA constituent is augmented from NC-1 – NC-3 bio-composite scaffolds, the porosities were amplified. Porosity classification is reinforced on the presence of visible pores with penetrability and external part of the porous prearrangement. It was recognized from scanning electron microscope examination that the attachment of Ga-HA guides to thicker pore fortifications with reduced porosity thus improved the mechanical features (Dan et al., 2016). Since a superior thickness of a bio-composite scaffold usually direct to greater mechanical constancy, a noteworthy porosity affords a beneficial biological background. An evenness between the porosity and breadth for a bio-composite scaffold must be documented for the certain claim.

3.5. Swelling studies

Swelling outcomes of equipped bio-composite scaffolds have been depicted in Fig. 4B. As it can be demonstrated from the consequences that with the up-regulating concentrations of Ga-HA, the swelling aptitude was fortified. This may because of the pore size, interconnecting positions and scaffold capacity. Swelling thus exploits the interior surface area of the scaffold. Bio-composite scaffolds offered a greater quality and allow it accessible for nutrients from culture media proficiently (Hasan et al., 2018).

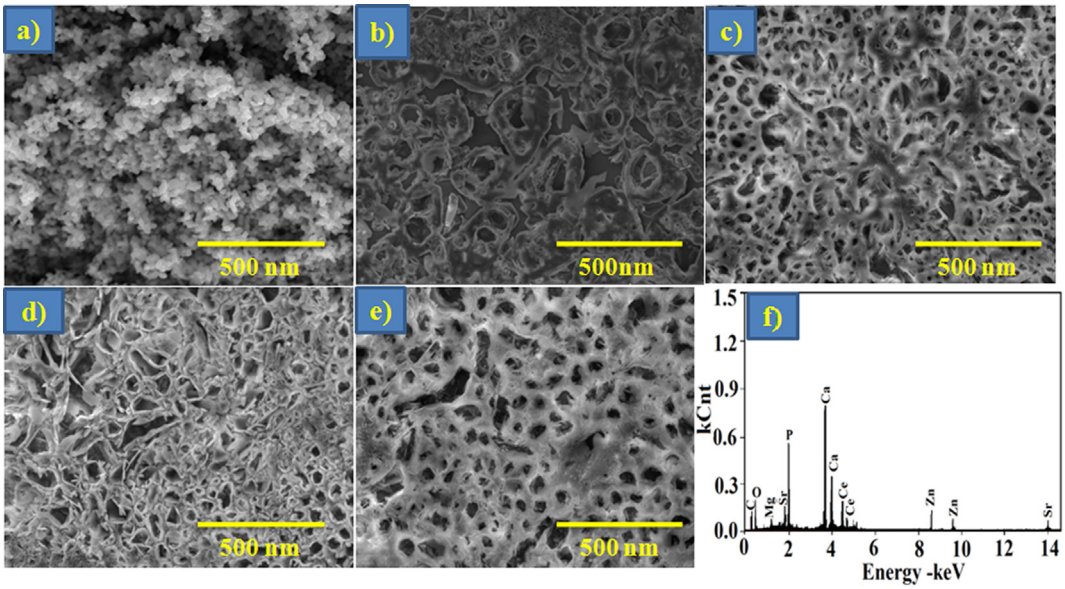

Fig. 3 SEM images of (a) Ga-HA (b) P-C (c) NC-1 (d) NC-2 (e) NC-3 and (f) EDX spectrum of NC3 nanocomposites. Fig. 3 establishes the SEM photomicrographs of the arranged composite samples. In pure Ga-HA nanoparticles displays spherical shape with particle sizes extending from ~70–100 nm (Fig. 3a), exposed interrelated pores (Fig. 3b-d). As it can be experiential in Fig. 3(c-e), the upsurge in the Ga-HA constituent leads to the expansion in the quantity of pores.

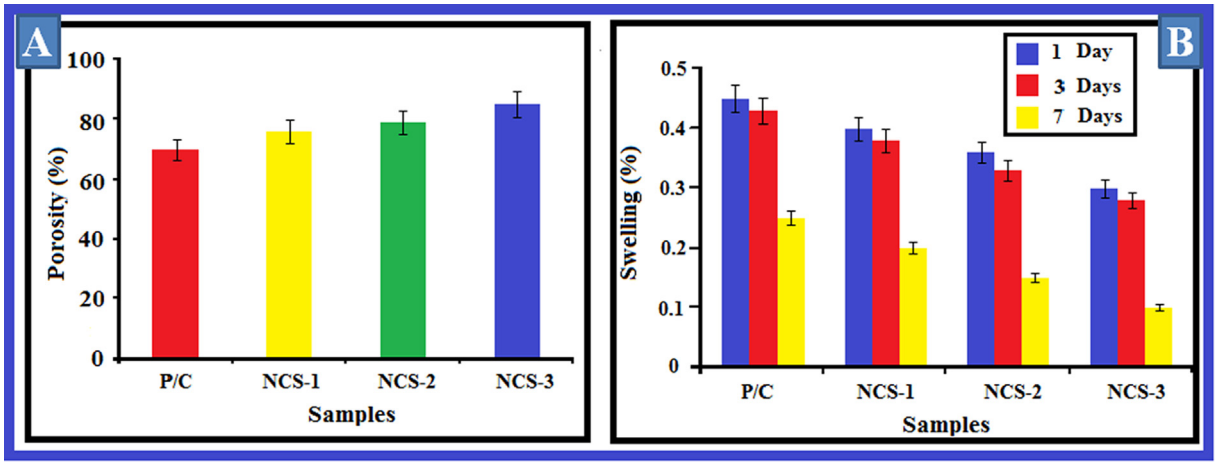

Fig. 4 (A) Porosity and (B) Swelling ratio of nanocomposites. The porosity of the organized Ga-HA/C/P scaffolds is pragmatic in Fig. 4A When the Ga-HA constituent is augmented from NC-1, NC-2, NC-3 bio-composite scaffolds, the porosities were amplified. Fig. 4B shows the swelling outcomes of equipped bio-composite scaffolds. As it can be demonstrated from the consequences that with the up-regulating concentrations of Ga-HA, the swelling aptitude was fortified. Values are depicted as mean ± SD of triplicate values analyzed by one was ANOVA subsequently DMRT test.

3.6. Mechanical properties

The power-driven characteristics of the bio-composite scaffold is a supplementary critical feature that was intentional for orthopedic submissions. Bio-composite scaffolds necessitate appropriate mechanical features to regulate their appearances during surgical imbedding and additionally to avert tissue strain or satisfying succeeding to implantation. Meanwhile bio-composites shaped from natural chitin and pectin is flat and delicate, they may not harvest the desirable mechanical structures afterward culturing cells following to establishment. The apatite reinforces bio-composite scaffolds and in this circumstance compressive robustness and modulus of the bio-composite scaffolds were improved with cumulative concentrations of Ga-HA constituent, which was depicted in Fig. 5A.

3.7. Deterioration analysis

Fig. 5B exemplifies the corrosion of nanocomposites. The consequences exposed that the mass obliteration was negligible in all the bio-composites. The mass loss rates was observed in all the scaffolds at lesser than 20% after 1 month. The deteriora-

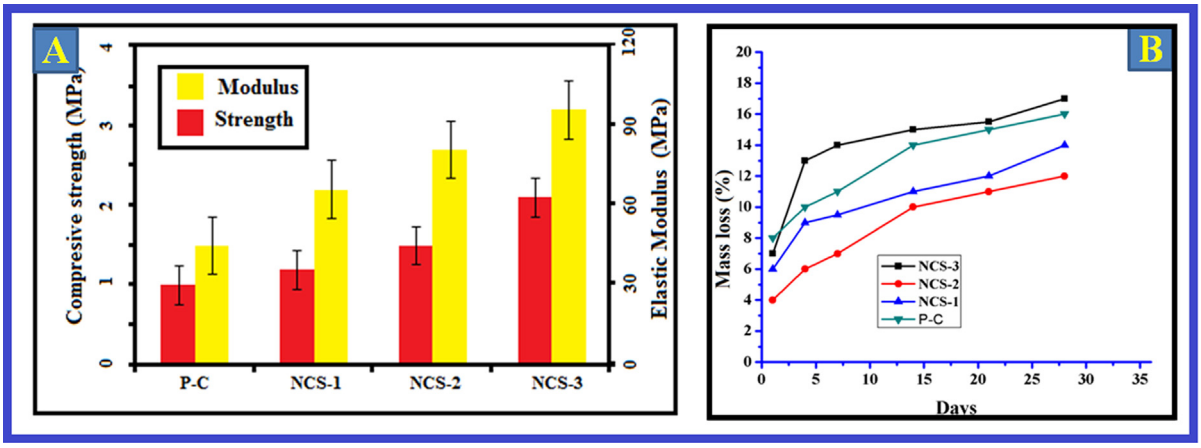

Fig. 5 (A) Mechanical properties and (B) Deterioration of nanocomposites. The apatite reinforces bio-composite scaffolds and in this circumstance compressive robustness and modulus of the bio-composite scaffolds were improved with cumulative concentrations of Ga-HA constituent, which was depicted in Fig. 5A. Fig. 5B exemplifies the corrosion of nanocomposites. The consequences exposed that the mass obliteration was negligible in all the bio-composites. The deterioration amount of fresh chitin was higher than the bio-composites. Values are depicted as mean ± SD of triplicate values analyzed by one was ANOVA subsequently DMRT test.

tion amount of fresh chitin was higher than the bio-composites. Pectin and chitin could be abridged by lysozyme contemporary in the human body. Preceding studies described that the biomolecules of the scaffold can experience degradation into small molecules in the occurrence of lysozyme. The outcomes of this present study exposed worsening rate of bio-composites was condensed with the attachment of Ga-HA element into the scaffolds representing adding of Ga-HA can modify the deprivation rate in composite scaffolds (Govindaraj et al., 2017).

3.8. Cell feasibility and augment analysis

In present study it was initiated that NIH3T3 and MG-63 cells were viable in existence of Ga-HA/C/P nanocomposite frameworks after 24 & 48 hrs throughout the experimentation phase that was demonstrated in (Fig. 6). These consequences recommended that cell viability was not affected by the supplementation of Ga-HA. When compared to the control cells, Ga-HA administered cells demonstrated the improved cell feasibility, it suggests that the Ga-HA was enhance the growth of NIH3T3 and MG-63 cells. DAPI staining was completed to display the cell add-onto the nanocomposite scaffolds and their propagation upon bonding with the rafts (Fig. 7). It was clearly suggests that the Ga-HA was noticeably improve the propagation of NIH3T3 and MG-63 cells when compared to control. Present statistics evidently exhibited the aptitude of scaffold to entice cells near to it and deviation on rafts or scaffolds. The cell enlargement and propagation aptitude of scaffold will aid the cells to diplomat and multiply in vivo.

3.9. In-vivo histological evaluation

3.9.1. H&E staining

The entrenched side of bone was repossessed to examine histologically for the assessment of newly shaped bone tissue. This stood well categorized and demonstrated by contrast with control (Rat deprived of implantation) by means of two dissimilar histopathological staining's such as H&E (Hematoxylin and Eosin) and MT staining (Masson-Trichrome). Fig. 8 portrays the histological segments of H&E discoloration. The development of new bone tissues subsequent to implacement is demonstrated from the segments. In controls, the osteoclasts survival in the bone medium are gotten as violet stained domain as designated by yellow shafts while the white circumstantial specified the occurrence of connected tissues. After 24 hr, 2nd week and 4th week of implantation, there was no indication for the development of new bone cells in the normal group.

After the implacement with Ga-HA/C/P scaffold age, the establishment of new bone is experiential with red discoloration and connecting tissues blemished white in the circumstantial (Shea et al., 2000; Zhu et al., 2020). The shady blue color specified by white arrow displays the occurrence of mellowed bone cells. With the upsurge in time phase i.e., from 2nd to 4th week, the mellowed bones fashioned the new bone cells deprived of the occurrence of osteoclasts and also the graft did not to harvest any clinical contagions counting tumors or inflammation.

3.9.2. Masson trichrome (MT) staining

The MT staining displayed the establishment of new bone tissues over osteoblast difference as showed in Fig. 9. In control groups, the amount of osteoid and osteoblast cells is designated in yellow and red color projectiles correspondingly. The spheres with minor white color signify osteoids and the progress of osteoids distinguishing to osteoblasts are characterized in huge spheres. Though afterward 4th week of surgery, there was nope new bone tissue development observed in the imperfection sideways of the control group, while in the Ga-HA/C/P managed group, the bony trabeculae construction is characterized with dark blue stain. Furthermore, the dominant cores of hardened cartilage shadowed by new bone development was experiential as shady blue at all time opinions. After 1 day of establishment, the new bone foundation was minutes associated with other periods such as 2nd and 4th week of imbedding. After the 4th week, more influential blue color was perceived(Qiu et al., 2020; Dantas et al., 2011) represent-

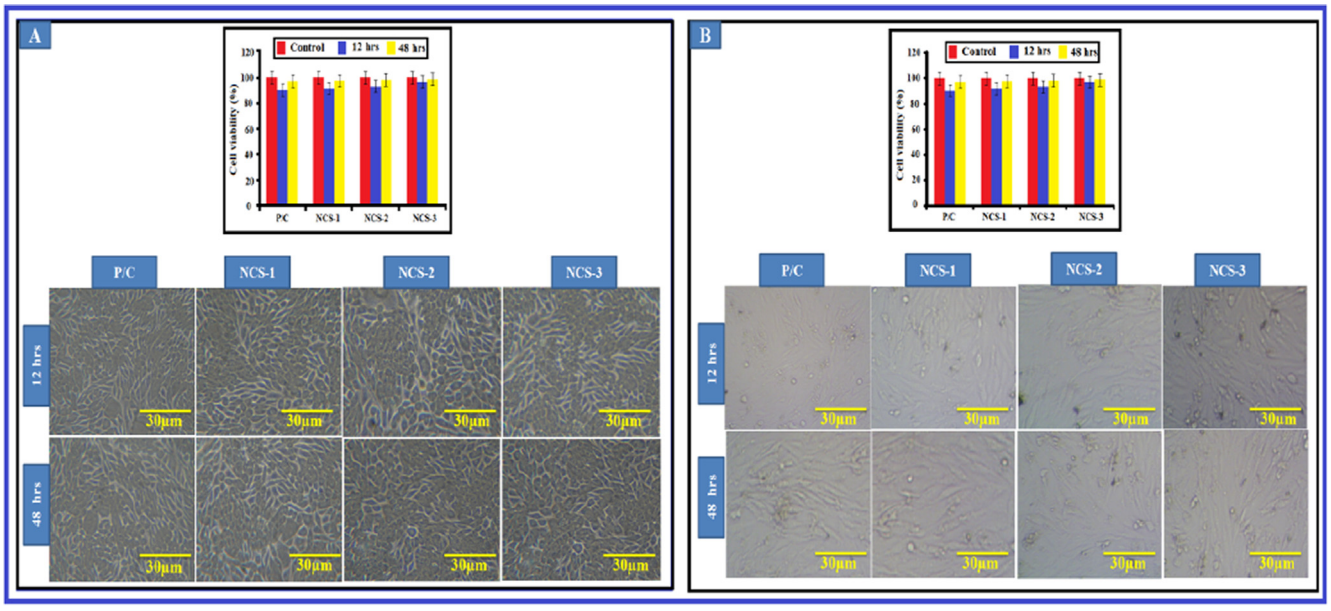

Fig. 6 Viability of nano-composites with different cell lines (A) NIH3T3 cells and (B) MG-63 cells. The cell viability of Ga-HA/C/P exposed NIH3T3 and MG-63 cells were demonstrated in Fig. 6. These consequences recommended that cell viability was not affected by the supplementation of Ga-HA/C/P. Values are depicted as mean ± SD of triplicate values analyzed by one was ANOVA subsequently DMRT test.

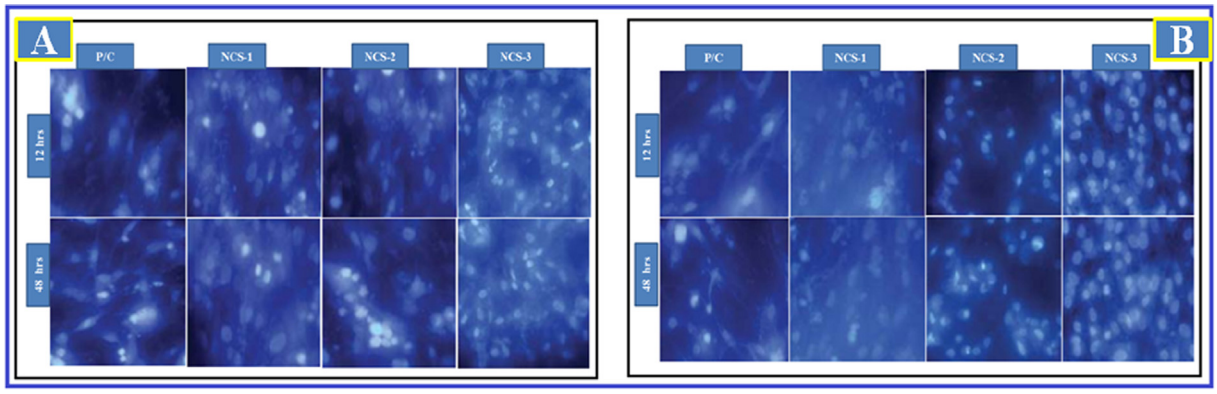

Fig. 7 Cell attachment on nano-composites with different cell lines (A) NIH3T3 cells and (B) MG-63 cells. DAPI staining was displayed that the Ga-HA/C/P exposed cells were noticeably improved the propagation of NIH3T3 and MG-63 cells when compared to control.

ing that the newly designed bone by osteoblast difference was improved by the Ga-HA/C/P scaffold grafting.

3.9.3. X-ray image examination

The alteration in the curative of imperfection side between the control and implanted clusters with Ga-HA/C/P scaffold assemblages were further long-established by X-ray image analysis (Fig. 10 A and B). In current study, we established that the osteoblast difference of innate bone was not exaggerated by our fictional raft or scaffold. The automatically shaped blemish side did not restore even after 4th week in normal. Though, after establishment with invented scaffold, the imperfection side was enclosed completely with mellowed bone and the location of imbedding was rehabilitated after 4th week of establishment. From these consequences, it is vibrant that fictitious scaffold was gifted to simplify the healing procedure of the bone. In adding, this scaffold persuaded bone development through the osteogenic difference in-vivo.

4. Discussion

The aptitude of artificial or natural polymeric scaffolds to sustenance the assault of cells from adjacent tissues is a limitation for tissue engineering. Third dimensional permeable polymer frameworks augment bone renaissance via generating and upholding an interplanetary space that simplifies predecessor cell relocation, propagation and difference (Shalumon et al., 2015; Gong et al., 2018; Ralte, 2014; Kee Jo et al., 2015). In present exploration, porous chitin assemblies were molded by freezing and lyophilizing chitosan–acetic acid solution in appropriate molds. Throughout the cold practice, ice crystals nucleate from solution and raise adjacent to the lines of

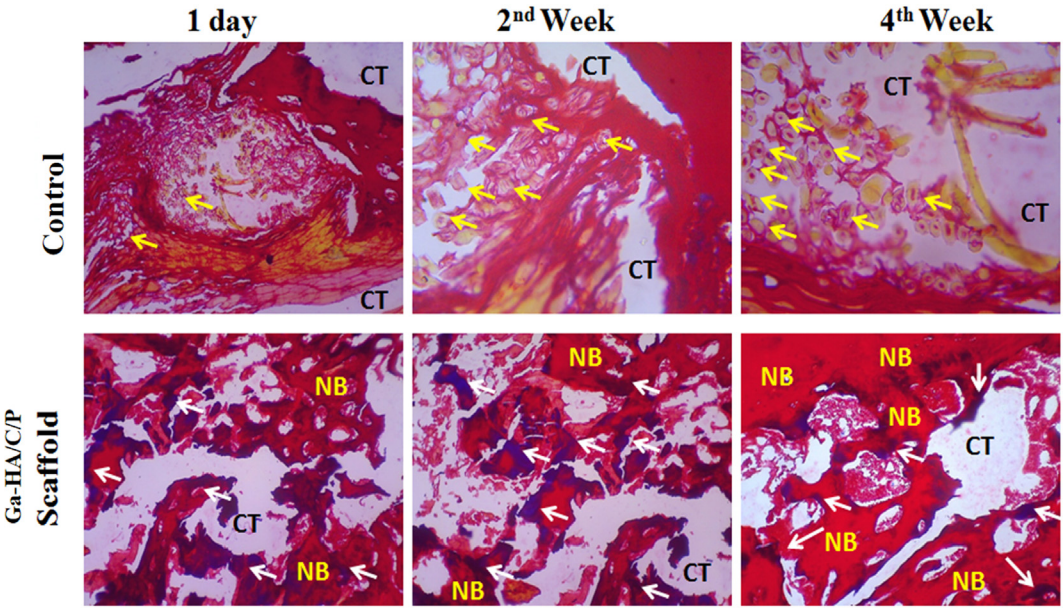

Fig. 8 H&E staining of experimented tissue without implantation (Control) and after implantation with Ga-HA/C/P scaffold on day 1, week 2 and week 4. Yellow arrow- Osteoblasts; White arrow- Matured bone cells; CT- Connective tissues; NB- New bone. Fig. 8 portrays the histological segments of H&E stained bone tissues. In controls, the osteoclasts survival in the bone medium are gotten as violet stained domain as designated by yellow shafts while the white circumstantial specified the occurrence of connected tissues. After 24 hr, 2nd week and 4th week of implantation, there was no indication for the development of new bone cells in the normal group.

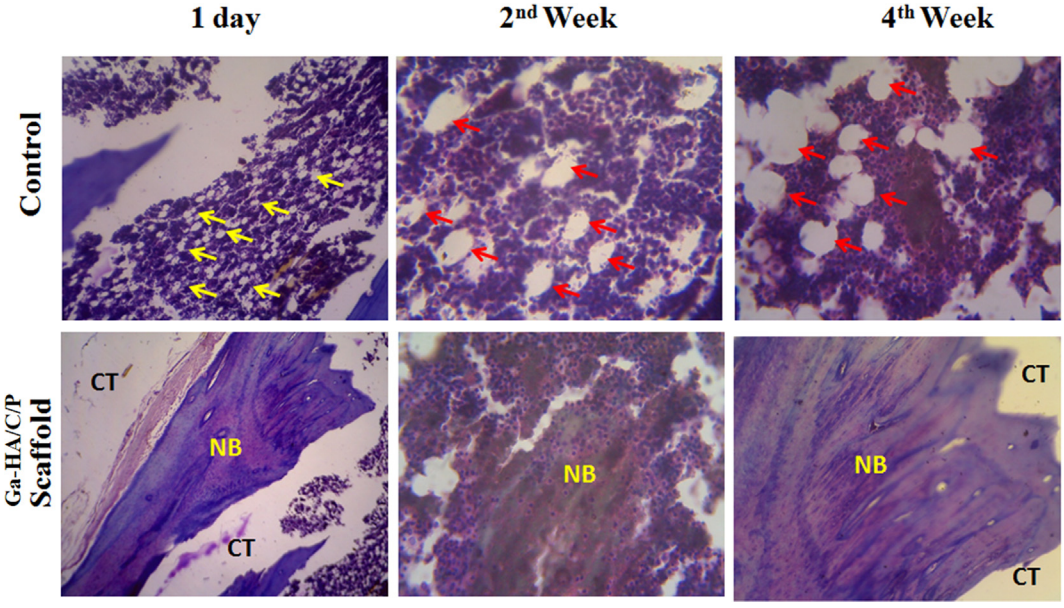

Fig. 9 MT staining of experimented tissue without implantation (Control) and after implantation with Ga-HA/C/P scaffold after day 1, week 2 and week 4. Yellow arrow- Osteoids; red arrow- Osteoblast cells; CT- Connective tissues; NB- New bone. The MT staining displayed the establishment of new bone tissues over osteoblast difference as showed in Fig. 9. In control groups, the amount of osteoid and osteoblast cells is designated in yellow and red color projectiles correspondingly. After 1 day of establishment, the new bone foundation was minutes associated with other periods such as 2nd and 4th week of imbedding. After the 4th week, more influential blue color was perceived representing that the newly designed bone by osteoblast difference was improved by the Ga-HA/C/P scaffold grafting.

updraft gradients. Elimination of the chitosan acetate salt from the ice crystal point and succeeding ice elimination by lyophilization produces an absorbent factual whose normal pore size is measured by fluctuating the freezing rate and henceforth the ice crystal extent. Pore alignment can be absorbed by regulating the geometry of thermal inclines in molds through subzero. The existence of apatite quartzes in three-dimensional polymer generates an ambience atmosphere

Fig. 10 X-ray images of (A) the surgical rat without any treatment and (B) Ga-HA/C/P implanted rat after 4th week of implantation. The alteration in the curative of imperfection side between the control and implanted clusters with Ga-HA/C/P scaffold assemblages were further long-established by X-ray image analysis (Fig. 10 A and B). The automatically shaped blemish side did not restore even after 4th week in control but in the Ga-HA/C/P scaffold administration.

for osteoconductive. The procedure of establishing apatite crystals through double diffusion is comparable to bone apatite development because of the attendance of phosphate ions in the liquid. Once a scaffold is entrenched, it interrelates with body liquid and forms a preliminary calcium composite and after that apatite construction, due to the occurrence of phosphate ions in the fluid (Zhao et al., 2003; Feng et al., 2019; Ding et al., 2019). In the current investigation, when the rafter is positioned in between phosphorous and calcium solutions in the compartment, the dispersion of ions takes place from the space of phosphorus ions near to the cavity of calcium ions and vice-like. The chitosan formulates a gel in the incidence of calcium ions and forms calcium multiplexes. These developments further intermingle with phosphate ions that long-winded into the sponge and form perilous nucleus size for nucleation and afterward hydroxyapatite nano-crystals are shaped. The confession of bone-like apatite on polymer medium in replicated body liquid as designated by biomimetic method (Manjubala et al., 2006; Yamaguchi et al., 2001; Falini et al., 2000; Puajindanetr et al., 1994).

SEM images of present study denotes chitosan fashioned by drying (freeze) are exposed in Fig. 3. A regular microporous assembly is experiential on the surface and an unvarying consistent open pore microstructure is detected in the section of the sponge. The assessment of the mineralization of the frameworks as exhibited in image, displays after a 3 hr period, the calcium phosphate mineral shelters the exterior and is erratically dispersed. The mineral is extra organized when the mineralization is agreed out for a lengthier phase. In some areas of the platform, the apatite gemstones are existing in cluster form of indicators. On the opening ramparts some agglomerates of spherical or spine-structured apatite, chitin and pectin crystals are experiential that are neither consistently dispersed nor layering the pore wall totally, as observed from Fig. 3. A comparable reflection was described by preceding studies in that there was none development of octa calcium phosphate pragmatic on the phosphate adjacent of the thin pictures in the dispersal procedure (Jonathan et al., 1999; Liu et al., 2018). The phase steadiness of the mineral bonds on the scaffolds, the scaffold mineralized for 2 days was ultrasonicated for 3 hr and the mineral credits discrete were poised cautiously, with subsequent air-dry and then heated up in air around 700 °C for about 12 hr. Current work coincide with the preceding work in which temperature was testified to augment the crystallinity of apatite and no further thermal point fluctuations aroused (Chavda et al., 2009; Guyton, 1977). The FT-IR peaks features of chitin, pectin-chitin for carbon-oxygen, carbon-hydrogen and amide cluster are extant in the spectrum. The allocation of peaks of pectin-chitin, Ga-HA are enumerated in Table 1. The peak at 1610 and 1396 cm^{-1} is because of the amide carbonyl stretch of chitin and pectin sharp peaks at 3428 and 2919 cm^{-1} is allocated to chitosan and apatite. The peak at 1635 cm^{-1} reduced in the mineralized scaffolds, demonstrating the communication of the amine on the chitosan and phosphates in the solution (Oates et al., 2007). The FT-IR examination in amalgamation with XRD study evidently designated the development of Ga-HA in the chitosan and pectin scaffold. The apatite fashioned was clean and no further phases of were shaped. This displays the possibility of establishment of HA nano-crystals, concerned along with the pore frequencies at ambience circumstances. Different nanocomposites viability was measured in which no toxic outcomes were noticed with mineralized samples via unswerving interaction of the material with NIH3T3 cells and MG-63 cells. Light microscopic photographs for mineralized chitosan and pectin scaffolds for 48 hr are displayed in Fig. 6 (a) and (b) correspondingly, and they display the regular, flat morphology of the cells representing that the two scaffolds are not toxic. The

cells multiplied in excess the outward of the framework and engaged their shape and an impenetrable coating of cell progress was experiential with the sample Fig. 6 (b).

In present work porosity and density of scaffolds of chitin and pectin were augmented. This was coincided with previous work in which density upsurges, while the porosity of super porous hydrogel composite reduced with upregulation in chitosan. Cumulative strength of chitosan prohibited the foams from absconding from the mixture and also it declines the pore size of hydrogel composite due the accretion of the chitosan at the margin of the pore (Lu et al., 2018; Li et al., 2018). Biocomposite of chitin and pectin impose suitable mechanical structures to normalize their entrances throughout surgical implanting. Our result correlate with hydrogel composite able to endure the pressure anticipated in the stomach throughout recurrent gastric reductions, particularly the housekeeper breakers. Preparation variables, like the sum of crosslinker, type of monomer, volume of blustering agent as well development variables all disturb the mechanical possessions of the hydrogel composite. The utmost pressure throughout the gastric shrinkage was stated to 60–70 cm water (Lu et al., 2018). Histological examines have also exposed the indication of the blood vessel cohort in a pattern in the boundaries of hydrogels allocated as angiogenic retort. Which was predetermined by preceding studies. Masson's trichrome staining also displayed there were additional osteocytes and collagen in the Ga-HA/C/P scaffolds. Therefore, the accumulation of pectin into chitosan/apatite scaffolds can improve osteogenesis through endorsing osteoblast variation and, in specific, mineralization. Previous works projects the same results (Feng et al., 2019).

5. Conclusion

In implication, the fortified Gallium-Apatite/chitin/pectin (Ga-HA/C/P) nanocomposites scaffolds (NCS) were well characterized by FT-IR, XRD and SEM-EDX presentations. NCSs were displayed to be tremendously permeable and impulsively stable with better density. Similarly, NCSs exposed enhanced swelling ability, lesser biodegradation percentage and progressive motor-powered strength. Additional cytotoxicity and cell devotion studies by means of NIH3T3 cells and MG-63 cell lines uncovered non-toxic and cells dedicated to pore exteriors of scaffolds. In vivo studies displayed advanced bone edifice through development of new bone cells and osteoblast alteration via the formation of NCSs. Fascinating consequences unruffled it can be depending that the prepared nanocomposite scaffolds own the requisites and exhibited great possibility for management of orthopedic conditions.

Declaration of Competing Interest

The authors declare no conflict of interest.

References

Banerjee, J., Vijayaraghavan, R., Arora, A., MacFarlane, D.R., Patti, A.F., 2016. Lemon juice based extraction of pectin from mango peels: waste to wealth by sustainable approaches. ACS Sustain. Chem. Eng. 4, 5915–5920.

Bouler, J.M., Pilet, P., Gauthier, O., Verron, E., 2017. Biphasic calcium phosphate ceramics for bone reconstruction: A review of biological response. Acta Biomater. 53, 1–12.

Bussy, C., Verhoef, R., Haeger, A., et al, 2008. Modulating in vitro bone cell and macrophage behavior by immobilized enzymatically tailored pectins. J. Biomed. Mater. Res. A 86 (3), 597–606.

Cassino, P.C., Rosseti, L.S., Ayala, O.I., Martines, M.A.U., Portugual, L.C., De Oliveira, C.G., Silva, I.S., Caldas, R.D.A., 2018. Potencial of different hydroxyapatites as biomaterials in the bone remodeling. Acta Cir Bras. 33, 816–823.

Chavda, H.V., Patel, C.N., Karen, H.D., 2009. Preparation and characterization of chitosan-based superporous hydrogel composite. J. Young Pharm. 1 (3), 199–204.

Chitambar, C.R., 2010. Medical applications and toxicities of gallium compounds. Int. J. Environ. Res. Public Health 7, 2337–2361.

Cui, L., Zhang, J., Zou, J., Yang, X., Guo, H., Tian, H., Zhang, P., Wang, Y., Zhang, N., Zhuang, X., Li, Z., Ding, J., Chen, X., 2020. Electroactive composite scaffold with locally expressed osteoinductive factor for synergistic bone repair upon electrical stimulation. Biomaterial. 230, 119617.

Dan, Y., Liu, O., Liu, Y., Zhang, Y.Y., Li, S., Feng, X.B., Shao, Z.W., Yang, C., Yang, S.H., Hong, J.B., 2016. Development of novel biocomposite scaffold of chitosan- gelatin/nanohydroxy apatite for potential bone tissue engineering applications. Nanoscale Res. Let. 11, 487–493.

Dantas, M.D.M., Cavalcante, D.R.R., Araújo, F.E.N., Barretto, S.R., Aciole, G.T.S., Pinheiro, A.L.B., Ribeiro, M.A.G., Lima-Verde, I. B., Melo, C.M., Cardoso, J.C., Albuquerque Júnior, R.L.C., 2011. Improvement of dermal burn healing by combining sodium alginate/chitosan-based films and low level laser therapy. J. Photochem. Photobiol. 105 (1), 51–59.

Ding, J., Zhang, J., Li, J., Li, D., Xiao, C., Xiao, H., Yang, H., Zhuang, X., Chen, X., 2019. Electrospun polymer biomaterials. Progress Polym. Sci. 90, 1–34.

Falini, G., Gazzano, M., Ripamonti, A., 2000. Control of the architectural assembly of octacalcium phosphate crystals in denatured collageneous matrices. J. Mater. Chem. 10, 535–538.

Feng, X., Li, J., Zhang, X., Liu, T., Ding, J., Chen, X., 2019. Electrospun polymer micro/nanofibers as pharmaceutical repositories for healthcare. J. Control Release 302, 19–41.

Gong, T., Liu, T., Zhang, L., Ye, W., Guo, X., Wang, L., Quan, L., Pan, C., 2018. Design redox-sensitive drug-loaded nanofibers for bone reconstruction. ACS Biomater. Sci. Eng. 4, 240–247.

Govindaraj D, Rajan M, Murugan, Munusamy A, Abdullah A. Alarfaj S. Kishor Kumar, Suresh Kumar S., 2017. The synthesis, characterization and in vivo study of mineral substituted hydroxyapatite for prospective bone tissue rejuvenation applications. Nanomed. Nanotech. Bio. Med 13(8), 2661-2669.

Govindaraj, D., Govindasamy, C., Rajan, M., 2017. Binary functional porous multi mineral–substituted apatite nanoparticles for reducing osteosarcoma colonization and enhancing osteoblast cell proliferation. Mater. Sci. Eng. 79, 875–885.

Govindaraj, D., Govindasamy, C., Rajana, M., 2017. Binary functional porous multi mineral– substituted apatite nanoparticles for reducing osteosarcoma colonization and enhancing osteoblast cell proliferation. Mater. Sci. Eng. 79, 875–885.

Guolin, H., Jeffrey, S., Kai, Z., Xiaolan, H., 2012. Application of ionic liquids in the microwave-assisted extraction of pectin from lemon peels. J. Ana. Method Chem. 2012,. https://doi.org/10.1155/2012/302059 302059.

Gurzawska, K., Svava, R., Jørgensen, N.R., Gotfredsen, K., 2012. Nanocoating of titanium implant surfaces with organic molecules. Polysaccharides including glycosaminoglycans. J. Biomed. Nanotechnol. 8 (6), 1012–1024.

Guyton, A.C., 1977. Basic human physiology: normal function and mechanisms of disease. Philadelphia: W.B. Saunders Co. 2, 662–664.

Hannink, G., Arts, J.J.C., 2011. Bioresorbability, porosity and mechanical strength of bone substitutes: What is optimal for bone regeneration?. Injury Int. J. Care Injured. 42, S22–S25.

Hasan, A., Waibhaw, G., Saxena, V., Pandey, L.M., 2018. Nano-biocomposite scaffolds of chitosan, carboxymethyl cellulose and silver nanoparticle modified cellulose nano whiskers for bone tissue engineering applications. Int. J. Biol. Macromol. 111, 923–934.

Jonathan, Z.K., Samuel, M.H., Katherine, A.M.C., 1999. Improved mechanical properties of chitosan fibres. J. Appl. Polym. Sci. 72, 1721–1732.

Kee Jo, Y., Choi, B., Zhou, C., Soo Ahn, J., Ho Jun, S., Joon Cha, H., 2015. Bioengineered mussel glue incorporated with a cell recognition motif as an osteostimulating bone adhesive for titanium implants. J. Mater. Chem. B. 3, 8102–8114.

Kokkonen, H.E., Ilvesaro, J.M., Morra, M., Schols, H.A., Tuukkanen, J., 2007. Effect of modified pectin molecules on the growth of bone cells. Biomacromolecules 8 (2), 509–515.

Kurtjak, M., Vukomanović, M., Kramer, L., Suvorov, D., 2016. Biocompatible nano-gallium/hydroxyapatite nanocomposite with antimicrobial activity. J. Mater. Sci. Mater. Med. 27, 170–183.

Lee, S.H., Lee, J.H., Cho, Y.S., 2014. Analysis of degradation rate for dimensionless surface area of well-interconnected PCL scaffold via in-vitro accelerated degradation experiment. Tissue Eng. Regen. Med. 11, 446–452.

Li, S., Dong, S., Xu, W., Tu, S., Yan, L., Zhao, C., Ding, J., Chen, X., 2018. Antibacterial hydrogels. Adv. Sci. 5 (5), 1700527.

Liu, H., Cheng, Y., Chen, J., Chang, F., Wang, J., Ding, J., Chen, X., 2018. Component effect of stem cell-loaded thermosensitive polypeptide hydrogels on cartilage repair. Acta Biomater. 73, 103–111.

Lu, Y., Li, L., Zhu, Y., Wang, X., Li, M., Lin, Z., Hu, X., Zhang, Y., Yin, Q., Xia, H., Mao, C., 2018. Multifunctional copper-containing carboxymethyl chitosan/alginate scaffolds for eradicating clinical bacterial infection and promoting bone formation. ACS Appl. Mater. Interfaces. 10 (1), 127–138.

Manjubala, I., Scheler, S., Bossert, J., Jandt, K.D., 2006. Mineralisation of chitosan scaffolds with nano-apatite formation by double diffusion technique. Acta Biomater. 2, 75–84.

Melnikov P, Teixeira AR, Malzac A, deB M. Coelho, 2009. Gallium-containing hydroxyapatite for potential use in orthopedics. Mater. Chem. Phys. 117, 86-90.

Mohamed, S., Hasan, Z., 1995. Extraction and characterization of pectin from various tropical Agro wastes. ASEAN Food J. 10, 43–50.

Morra, M., Cassinelli, C., Cascardo, G., et al, 2004. Effects on interfacial properties and cell adhesion of surface modification by pectic hairy regions. Biomacromolecules 5 (6), 2094–2104.

Nayak, B., Misra, P.K., 2020. Exploration of the structural and dielectric characteristics of a potent hydroxyapatite coated gallium bioceramics for the forthcoming biomedical and orthopedic applications. Mater. Chem. Phys. 239, 121967.

Noreen, A., Nazli, Z.I., Akram, J., Rasul, I., Mansha, A., Yaqoob, N., Iqbal, R., Tabasum, S., Zuber, M., Zia, K.M., 2017. Pectins functionalized biomaterials; a new viable approach for biomedical applications: A review. Int. J. Biol. Macromol. 101, 254–272.

Oates, M., Chen, R., Duncan, M., Hunt, J.A., 2007. The angiogenic potential of three-imensional open porous synthetic matrix materials. Biomaterials 28, 3679–3686.

Pal, A., Paul, S., Choudhury, A.R., Balla, V.K., Das, M., Sinha, A., 2017. Synthesis of hydroxyapatite From Late scalcarifer fish bone for biomedical applications. Mater. Let. 203, 89–92.

Puajindanetr, S., Best, S., Bonfield, W., 1994. Characterisation and sintering of precipitated hydroxyapatite. Br. Ceram. Trans. 93, 96–99.

Qiu, H., Guo, H., Li, D., Hou, Y., Kuang, T., Ding, J., 2020. Intravesical hydrogels as drug reservoirs. Trends Biotechnol. 38 (6), 579–583.

Ralte, S., 2014. Histomorphology of Metaphysis of Proximal Tibia in Albino Rat. Austin. J. Anat. 2, 1010.

Shalumon, K.T., Lai, G.J., Chen, C.H., Chen, J.P., 2015. Modulation of Bone-Specific Tissue Regeneration by Incorporating Bone Morphogenetic Protein and Controlling the Shell Thickness of Silk Fibroin/Chitosan/Nanohydroxyapatite Core−Shell Nanofibrous Membranes. ACS Appl. Mater. Interfaces. 7, 21170–21181.

Shea, L.D., Wang, D., Franceschi, R.T., Mooney, D.J., 2000. Engineered bone development from a pre-osteoblast cell line on three-dimensional scaffolds. Tissue Eng. 6, 605–617.

Supova, M., 2015. Substituted hydroxyapatites for biomedical applications: A review. Ceram Int. 41, 9203–9231.

Tiedeman, J.J., Garvin, K.L., Kile, T.A., Connolly, J.F., 1995. The role of a composite, demineralized bone matrix and bone marrow in the treatment of osseous defects. Orthopedics. 18, 1153–1158.

Usman, A., Zia, K.M., Zuber, M., Tabasum, S., Rehman, S., Zia, F., 2016. Chitin and chitosan-based polyurethanes: A review of recent advances and prospective biomedical applications. Int. J. Biol. Macromol. 86, 630–645.

Wang, C., Wang, J., Zeng, L., Qiao, Z., Liu, X., Liu, H., Zhang, J., Ding, J., 2019a. Fabrication of electrospun polymer nanofibers with diverse morphologies. Molecules 24 (5), 834.

Wang, C., Feng, N., Chang, F., Wang, J., Yuan, B., Cheng, Y., Liu, H., Yu, J., Zou, J., Ding, J., Chen, X., 2019b. Injectable cholesterol-enhanced stereocomplex polylactide thermogel loading chondrocytes for optimized cartilage regeneration. Adv. Healthcare Mat. 8, (14) e190031.

Williams, D.F., 1999. Williams dictionary of biomaterials. Liverpool University Press, Liverpool.

Wu, G., Deng, X., Song, J., Chen, F., 2018. Enhanced biological properties of biomimetic apatite fabricated polycaprolactone/chitosan nanofibrous bio-composite for tendon and ligament regeneration. J. Photochem. Photobiol. 178, 27–32.

Yamaguchi, I., Tokuchi, K., Fukuzaki, H., Koyama, Y., Takakuda, K., Monma, H., et al, 2001. Preparation and microstructure analysis of chitosan/hydroxyapatite nanocomposites. J. Biomed. Mater. Res. 55, 20–27.

Yang, S., He, H., Wang, L., Jia, X., Feng, H., 2011. Oriented Crystallization of Hydroxyapatite by the Biomimic Amelogenin Nanospheres from the Self-Assemblies of Amphiphilic Dendrons. Chem. Commun. 47, 10100–10102.

Zhang, W., Xu, P., Zhang, H., 2015. Pectin in cancer therapy: A review. Trends Food Sci. Technol. 44, 258–271.

Zhang, J., Xu, W.R., Zhang, Y., Li, W., Hu, J., Zheng, F., Wu, Y., 2018. Liquefied chitin/polyvinyl alcohol based blend membranes: Preparation and characterization and antibacterial activity. Carbohydr. Polym. 180, 175–181.

Zhang, Y., Yu, J., Ren, K., Zuo, J., Ding, J., Chen, X., 2019a. Thermosensitive hydrogels as scaffolds for cartilage tissue engineering. Biomacromolecule. 20 (4), 1478–1492.

Zhang, Y., Liu, X., Zeng, L., Zhang, J., Zuo, J., Zou, J., Ding, J., Chen, X., 2019b. Polymer fiber scaffolds for bone and cartilage tissues engineering. Adv. Function Mat. 29 (36), 1903279.

Zhang, Y., Ding, J., Qi, B., Tao, W., Wang, J., Zhao, C., Peng, H., Shi, J., 2019c. Multifunctional fibers to shape future biomedical devices. Adv. Function. Mat. 29 (34), 1902834.

Zhao, F., Yin, Y., Lu, W.W., Leong, C., Zhang, W., Zhang, J., et al, 2003. Preparation and histological evaluation of biomimetic three-dimensional hydroxyapatite/chitosan–gelatin network composite scaffolds. Biomaterials 23, 3227–3234.

Zhu, T., Cui, Y., Zhang, M., Zhao, D., Liu, G., Ding, J., 2020. Engineered three-dimensional scaffolds for enhanced bone. Bioactive Material. 5 (3), 584–601.